

Hijacking of the Enterobactin Pathway by a Synthetic Catechol Vector Designed for Oxazolidinone Antibiotic Delivery in *Pseudomonas aeruginosa*

Lucile Moynié, Françoise Hoegy, Stefan Milenkovic, Mathilde Munier, Aurélie Paulen, Véronique Gasser, Aline L. Faucon, Nicolas Zill, James H. Naismith, Matteo Ceccarelli, Isabelle J. Schalk, and Gaëtan L.A. Mislin*

Cite This: <https://doi.org/10.1021/acsinfectdis.2c00202>

Read Online

ACCESS |

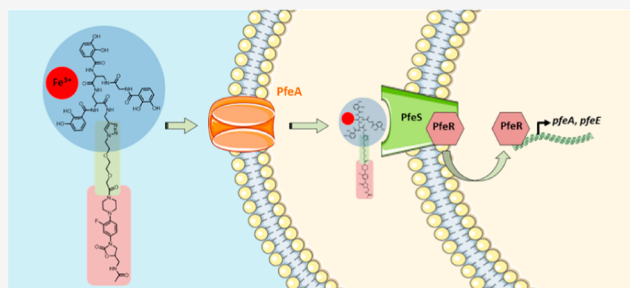
Metrics & More

Article Recommendations

Supporting Information

ABSTRACT: Enterobactin (ENT) is a tris-catechol siderophore used to acquire iron by multiple bacterial species. These ENT-dependent iron uptake systems have often been considered as potential gates in the bacterial envelope through which one can shuttle antibiotics (Trojan horse strategy). In practice, siderophore analogues containing catechol moieties have shown promise as vectors to which antibiotics may be attached. Bis- and tris-catechol vectors (BCVs and TCVs, respectively) were shown using structural biology and molecular modeling to mimic ENT binding to the outer membrane transporter PfeA in *Pseudomonas aeruginosa*. TCV but not BCV appears to cross the outer membrane via PfeA when linked to an antibiotic (linezolid). TCV is therefore a promising vector for Trojan horse strategies against *P. aeruginosa*, confirming the ENT-dependent iron uptake system as a gate to transport antibiotics into *P. aeruginosa* cells.

KEYWORDS: enterobactin, siderophore, linezolid, Trojan horse strategy, iron uptake, *Pseudomonas aeruginosa*



Pathogenic bacteria remain a potent threat to humans despite the discovery of antibiotics which had appeared to promise the end of bacteria as the cause of human diseases. This is because the accumulated use and misuse of antibiotics has led to the evolution of antibiotic-resistant bacterial strains. Continuing development of new antibiotic compounds and antibacterial strategies is crucial to avoid a return to the pre-antibiotic world, and there is particular concern over Gram-negative bacteria due to the paucity of new approaches. *Pseudomonas aeruginosa* is an opportunistic Gram-negative bacterium responsible for severe pulmonary infections affecting patients with cystic fibrosis and chronic obstructive pulmonary diseases.^{1,2} This pathogen is also common in infections of severe burns and often occurs in clinical HIV and other immunocompromised patients.^{3,4} *P. aeruginosa* is naturally resistant to many classes of antibiotics due to the low permeability of the outer membrane.⁵ The outer membrane in Gram-negative bacteria in general is a selective barrier that restricts the penetration of many xenobiotic compounds, not just antibiotics. The nutrient uptake systems act as selective openings in the bacterial envelope and have long been thought as a possible route for antibiotic uptake. This so-called Trojan horse strategy should ideally utilize an essential and metabolically unsubstitutable nutrient to have a significant

impact on bacterial proliferation. Iron is the best nutrient that meets these criteria.

The concentration of free Fe(III) in normal human fluids is estimated to be around 10^{-24} M, reflecting the inherent lack of bioavailability of the element. This presents a challenge for pathogenic bacteria where an Fe(III) concentration in the micromolar range was estimated to be optimal for bacterial proliferation.^{6,7} To surmount this challenge, bacteria have evolved with efficient uptake systems that are able to give them access to iron from their environment.⁸ One example is the ubiquitous siderophore-dependent iron transport systems. Siderophores are small Fe(III) chelating secondary metabolites secreted by bacteria, with diverse chemical structures and metal-to-ligand stoichiometries.^{9,10} The ferric complexes are next recognized by specific bacterial outer membrane transporters and imported back into the bacteria.^{11,12} The energy necessary for this active uptake through the outer membrane is provided by the TonB machinery and inner membrane proton-motive force.^{11–14} Some siderophores release iron in the bacterial periplasm, whereas other siderophores cross the inner membrane before delivering the iron. In both scenarios, iron release from siderophores involves a reductive process

Received: April 17, 2022

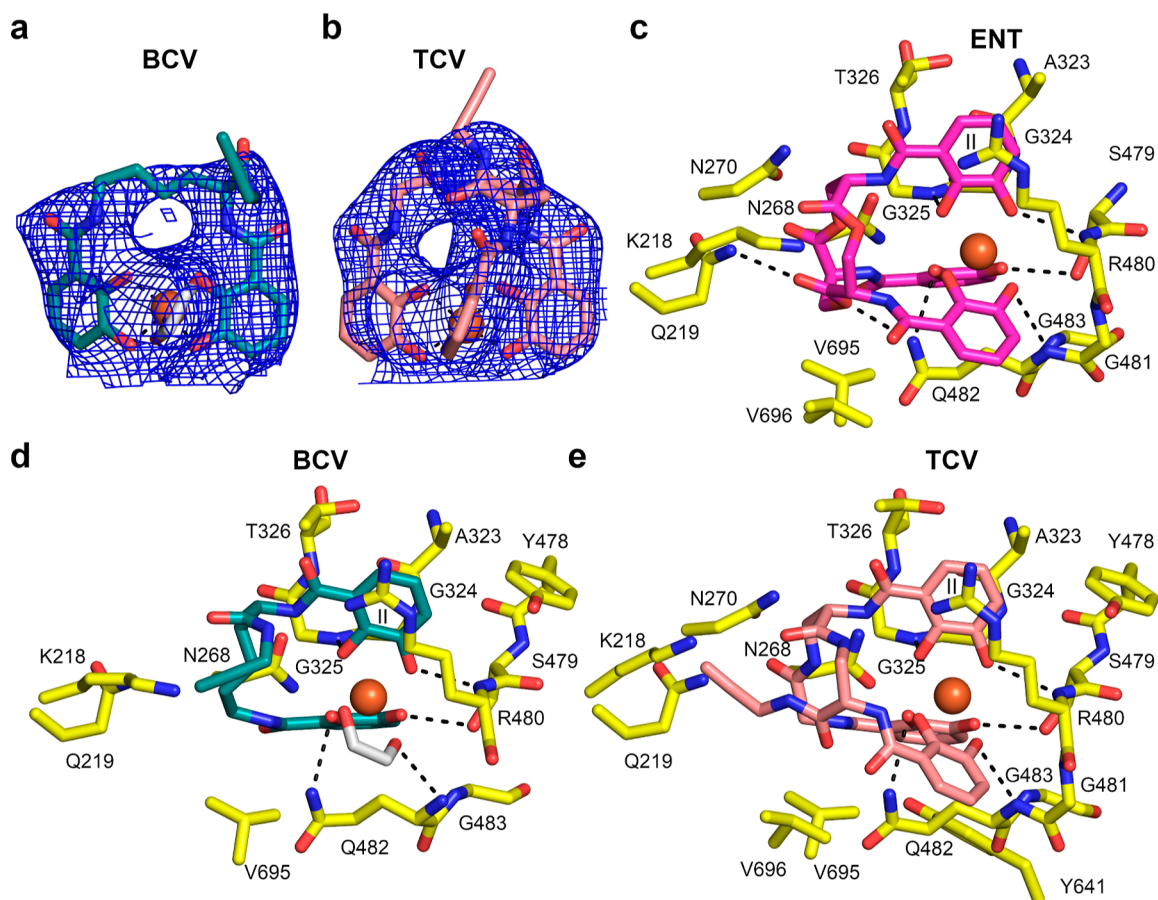


Figure 3. Structure of Fe³⁺-BCV and Fe³⁺-TCV in complex with PfeA. (a,b) Final 2F_o-F_c electron density map contoured at a 1σ level around Fe³⁺-BCV and Fe³⁺-TCV, respectively. Molecules are shown as sticks with carbon atoms colored in deep teal (BCV) or salmon (TCV), nitrogen in dark blue, and oxygen in red. Fe³⁺ is represented as an orange sphere. In the PfeA-Fe³⁺-BCV complex, one ethylene glycol molecule (white sticks) completes the coordination shell of the iron. (c-e) Comparison of the binding site of Fe³⁺-ENT (pink, from 6Q5E),³⁸ Fe³⁺-BCV, and Fe³⁺-TCV, respectively. Residues within 4.0 Å of the siderophores are displayed, and hydrogen bonds are shown as black broken lines.

extremity of the extracellular loops and a second deeper in the barrel located on the top of the plug domain.³⁸ The mechanism of translocation of ferric siderophore complexes through TBDT is still unclear, but the current model suggests that the binding of ferric ENT to PfeA triggers the interaction between the PfeA “TonB box” and the inner membrane TonB complex, which provides the energy needed for the conformation change of the plug domain and the translocation of the ferric siderophore complex through the transporter. Such a mechanism has been proposed for other TonB-dependent siderophore transporters.^{47,48}

Catechol vectors linked to oxazolidinones have shown activity against Gram-negative pathogens including *P. aeruginosa*.^{49,50} An improved knowledge of the molecular mechanisms involved in the uptake of catechol type siderophore-antibiotic conjugates across the outer membrane will enhance further development of next-generation conjugates. We report here how PfeA interacts with different synthetic catechol siderophore-antibiotic conjugates, BCV 4 and TCV 5 (bis- and tris catechol vectors, respectively)⁵¹ coupled to linezolid (inactive against *P. aeruginosa* when unconjugated). We have previously shown³⁹ that BCV 4 and TCV 5 both induce the expression of the proteins of the ENT-dependent iron uptake pathway (PfeA and PfeE) in *P. aeruginosa* cells.^{39,51} Here, BCV- and TCV-conjugates proved to be invaluable molecular tools to investigate, for the first time, the molecular

basis of the interaction of siderophore-antibiotic conjugates with the outer membrane transporter.

RESULTS AND DISCUSSION

BCV and TCV Interaction with the PfeA Transporter.

We determined the structure of PfeA-Fe³⁺-BCV and PfeA-Fe³⁺-TCV to be of 2.7 and 2.6 Å resolutions, respectively (Figures 3a,b, S1 and S2 and Table S1 in the Supporting Information). Both BCV 4 and TCV 5 bind to the PfeA first binding site located in the extracellular loops reported for ENT (Figures 3c-e, S1 and S2 in the Supporting Information). Two of the catecholate rings occupy the same position as rings 2 and 3 of ENT. Key hydrogen bonds involved in the recognition between the catecholates of ENT and Gly325, Ser479, Arg480, and Gln482 are conserved. In the Fe³⁺-TCV complex, the third catecholate slightly shifts toward Arg480 (relative to ENT) to accommodate the propargyl arm. The stacking interaction of Arg480 with catecholate 2 is preserved. The two last atoms of the propargyl group were not clearly defined in the electron density map and were assumed to be disordered due to mobility. However, based on the well-ordered portion, the propargyl group points to the surface of the protein (Lys218 of L2), which is slightly displaced compared to the Fe³⁺-ENT structure (Figure S1 in the Supporting Information). In the Fe³⁺-BCV complex, the iron coordination sphere is completed by interaction with a

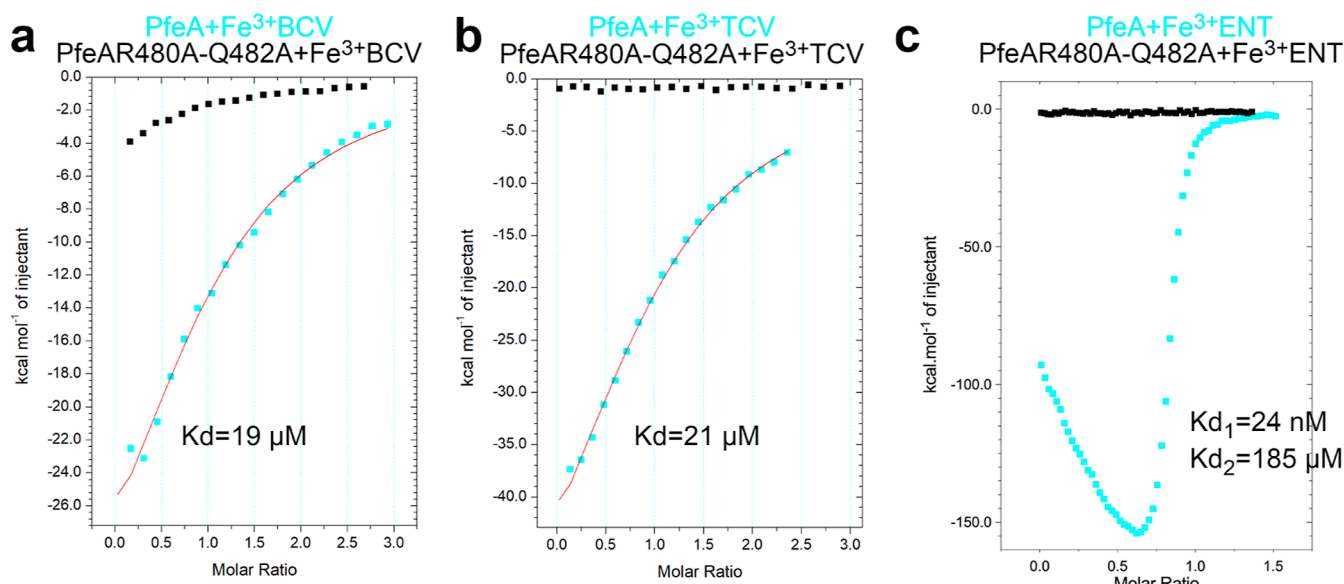


Figure 4. Comparison of the isothermal calorimetry titration of Fe^{3+} -BCV (a), Fe^{3+} -TCV (b), and Fe^{3+} -ENT (c) (shown for comparison but underlying data are previously reported³⁸) with PfcA (cyan) and mutants R480A-Q482A (black) shows that Fe^{3+} -BCV and Fe^{3+} -TCV bind to PfcA specifically. The heats of dilution measured from injection of the ligands into the buffer were subtracted and TCV and BCV titration have been fitted with a one-site interaction model instead of two binding sites.

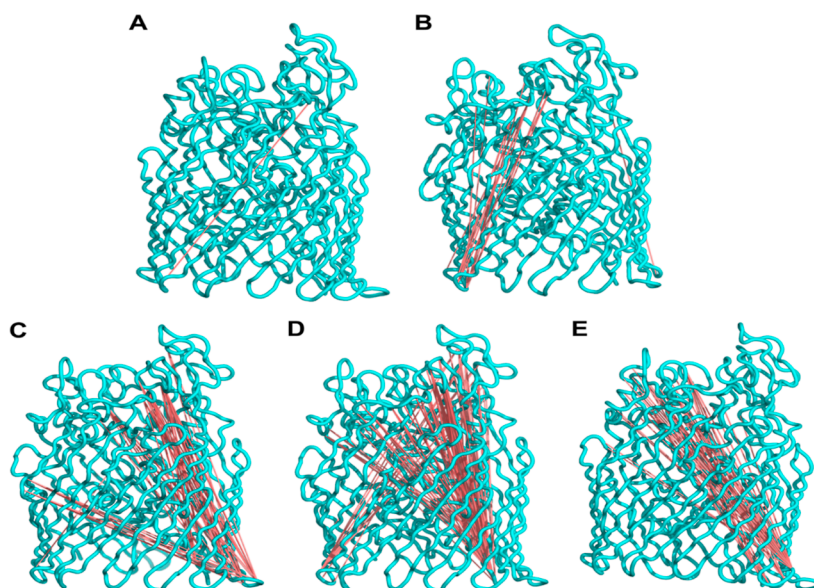


Figure 5. α -correlation (>0.5) of distant residue pairs in (A) empty PfcA, (B) PfcA R480A-Q482A, (C) PfcA- Fe^{3+} -ENT complex, (D) PfcA- Fe^{3+} -BCV complex, and (E) PfcA- Fe^{3+} -TCV complex.

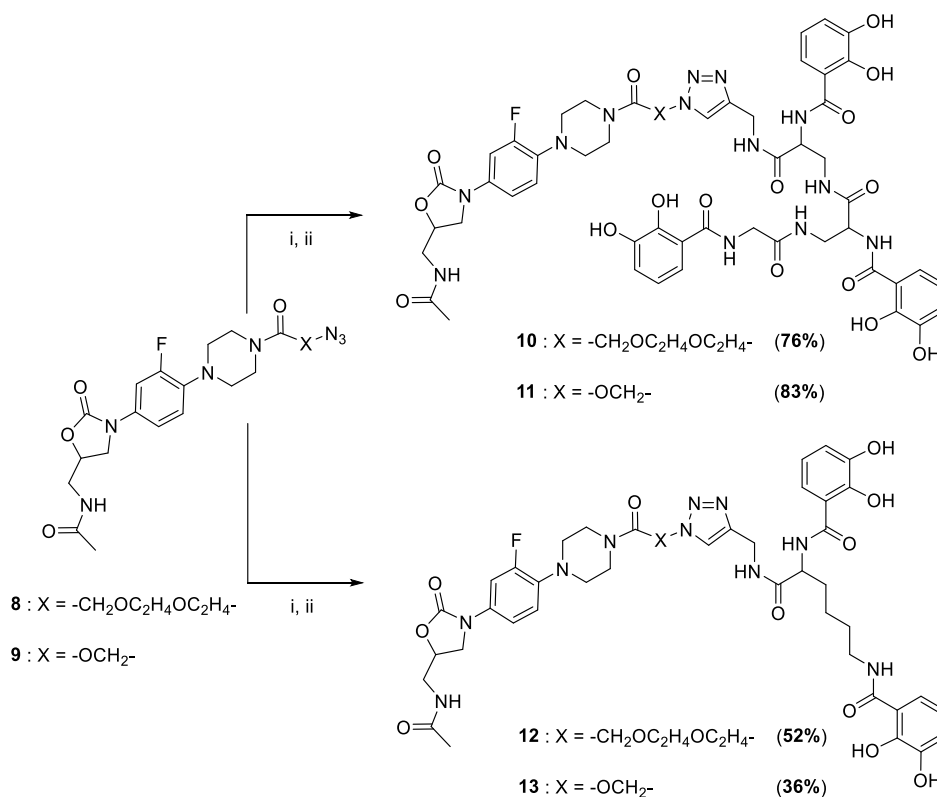
molecule of ethylene glycol from a buffer (seen in the PfcA- Fe^{3+} -azotochelin complex).³⁸ In the BCV ferric complex, the propargyl group also points to Lys218.

A previous thermodynamic analysis (isothermal titration calorimetry, ITC) of ENT titrated into PfcA showed a biphasic heat profile. Coupled to modeling studies, this was interpreted as two cooperating binding sites, one high affinity site (~ 30 nM) and one lower affinity site (~ 190 μM), within PfcA.³⁸ Titrations of both Fe^{3+} -BCV and Fe^{3+} -TCV into PfcA by ITC were best fitted to a single site-binding model with a much-reduced enthalpy (-50 to 60 kcal mol⁻¹) and lower affinity (19 μM for BCV and 21 μM for TCV) (Figures 4, S6 and S7, and Table S2 in the Supporting Information). ITC was repeated with a PfcA double mutant (R480A-Q482A) and

showed no binding for Fe^{3+} -TCV and considerably weaker binding for Fe^{3+} -BCV. These observations support the structural biology data that both catecholates bind to the first binding site of PfcA, which governs siderophore recognition but does so with a significant reduction in affinity compared to that of the native ligand.

Signaling through the Outer Membrane Promoted by BCVs and TCVs. Molecular dynamics (MD) simulations previously reported³⁸ suggest that upon binding of Fe^{3+} -ENT to PfcA, a signal transmits from extracellular loops to the N-terminal TonB box located in the periplasm.³⁸ This signal was indicated by means of a α correlation, a method that allows the detection of correlated motions between distant sites in proteins,^{52,53} which was performed in the same way as

Scheme 1. Synthesis of TCV–Oxazolidinone Conjugates 10 and 11 and of BCV–Oxazolidinone Conjugates 12 and 13; (i) 6 or 7, CuSO₄, Sodium Ascorbate, THF/H₂O, 20 °C; (ii) TFA/CH₂Cl₂, 20%, TIPS, EtOH, 20 °C



described in the Materials and Methods section of this work. The concerted motions between the binding site and the TonB box region were confirmed by a detailed analysis of crystallographic and simulation data where the chain of events leading to signal propagation was identified.³⁸ Here, judged by the $C\alpha$ correlation in the MD structures, both BCV 4 (Figure 5D) and TCV 5 (Figure 5E) mimic the ENT (Figure 5C) signal transmission pathway, in that they showed strongly correlated pairs of residues separated by an average distance of at least 50 Å connected via red lines (Figure 5C). In the empty transporter³⁸ and double mutant, there is no such correlation (Figure 5A,B, respectively).

The correlation between the different structures can be visualized in full detail plotting the $C\alpha$ -correlation among all pairs of residues as a function of their separation (Figure S8A–E in the Supporting Information). The long-distance signaling across different systems manifested in the rise of correlation above 50 Å, a distance comparable to the membrane thickness. Finally, the data are summarized in the form of a cumulative histogram (Figure S8F in the Supporting Information), which allows for the quantification of the effect counting the pairs with a correlation larger than 0.4 and with a separation larger than 50 Å. We see a clear difference between systems with weak signaling (empty and double mutant PfeA) and systems with strong signaling (ferric ENT, ferric BCV 4, and ferric TCV 5). Interestingly, the strongest signal is detected in the PfeA–Fe³⁺–TCV 5 complex.

Conjugation of Oxazolidinones with BCVs and TCVs. Since both 4 and 5 were bound by PfeA and appeared to stimulate TonB signaling, we synthesized BCV– and TCV–oxazolidinone compounds. Protected BCV 6 and TCV 7 were reacted with oxazolidinone azides 8 and 9⁵⁴ using a copper(I)-

catalyzed alkyne–azide cycloaddition.^{55,56} Deprotection of the catechol functions of the resulting compounds in the presence of TFA led to the expected conjugates 10 to 13 isolated in, respectively, 76, 83, 52, and 36% yield over two combined synthetic steps. In conjugates 10 to 13, vectors and antibiotics are connected through a 1,2,3-triazole moiety (Scheme 1). The linkers were selected since the use of these conjugates as molecular tools requires a stability of the conjugation all along the uptake and signaling process. We also selected these structures to investigate the effect of linkers of different sizes on the recognition of the conjugates and proteins involved in the uptake and signaling system.

Antibacterial Activity of Oxazolidinone Conjugates.

The oxazolidinone antibiotic family, of which linezolid serves as an example,⁵⁷ exerts its effect by binding to the ribosomal 50S subunit. In *S. aureus*, the conjugates 10 (MIC = 64 μM) and 11 (MIC = 16 μM) retained some of the antibiotic activity of linezolid (MIC = 4 μM), showing that (1) the conjugates were transported into the *S. aureus* cytoplasm and (2) oxazolidinone linked to the vector can still bind but with a lower activity than the oxazolidinone alone presumably due to the presence of the siderophore. Conjugates 10 to 13 had no significant antibiotic activity on *P. aeruginosa* (MIC > 64 μM), suggesting that these molecules are unable to interact with their target and/or unable to reach the ribosome in this pathogen (Table S3 in the Supporting Information).

Interaction of Catechol Vector–Oxazolidinone Conjugates with the PfeA Transporter. The X-ray structure between PfeA and the linezolid conjugates 10, 11, 12, and 13 showed the presence in the transporter first binding site of BCV and TCV moieties, but no density was observed for the antibiotic conjugate (Figure S3 in the Supporting Informa-

tion). The entire conjugate was observed with good electron density at the crystallographic interface between three molecules of PfeA in the complex structure with **11** (Figure S4 in the Supporting Information). This finding, consistent with analytical data, suggests that the conjugate was not degraded but rather disordered due to flexibility. Of course, the molecule bound at the crystal interface is a crystallization artifact and does not inform about transport. If the antibiotic is disordered, then the conjugate does not alter the recognition by PfeA (Figures S1, S2, and S5 in the Supporting Information). In the TCV conjugates **10** and **11**, a water molecule has been identified between two of the catecholates making hydrogen bonds with Arg480 and two amides of the TCV backbone (Figure S5e,f in the Supporting Information). A close inspection of the TCV complex map suggests that a water molecule may occupy the same position in the structure but was not included as this was ambiguous. The titrations of Fe^{3+} -TCV **5** and Fe^{3+} -BCV **4** into PfeA by ITC show a much weaker binding compared to that of Fe^{3+} -ENT. The addition of the linezolid connected by a short linker (TCV-L6 **11** and BCV-L6 **13**) has little additional effect (38 and 20 μM , respectively), but a longer linker (TCV-L5 **10** and BCV-L5 **12**) does further reduce binding (100 and 37 μM) (Figure S6 and Table S2 in the Supporting Information). MD simulations of PfeA in complex with ferric TCV-L6 **11** suggest that very fast after the initial equilibration, TCV-L6 **11** moves into the second binding site (Figure S9 in the Supporting Information). This suggests that when merged, the first and the second binding sites could host molecules significantly larger than the ENT if the initial interaction between PfeA and the molecule induces a proper signal. By superimposing the poses of TCV-L6 on PfeA sampled with MD simulations (Figure 6), we see

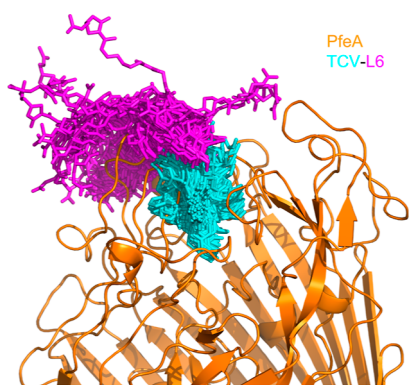


Figure 6. Dynamics of TCV-L6 **11** interaction with PfeA as extracted from MD simulations. The linezolid part of the molecule is shown in magenta, the TCV part is shown in cyan, and PfeA is given in orange. The linezolid part fluctuates much more than the TCV part and it can be considered disordered, explaining the difficulties to catch it with XRD.

that the linezolid part fluctuates much more than the TCV part. Thus, it can be considered disordered, explaining the difficulties to catch it with X-ray diffraction (XRD).

Presence of the TCV–Oxazolidinone Conjugates in the Growth Media of *P. aeruginosa* Efficiently Promotes the Induction of the Expression of PfeA and PfeE. Crystallography and ITC indicate that conjugates **10** to **13** bind their cognate outer membrane transporter PfeA. However, we were unable to carry out radioactive iron (^{55}Fe) uptake assays with sufficiently strong signal-to-noise

ratio (SNR) to confirm transport. The SNR arises from precipitation of iron-loaded conjugates. Consequently, we investigated whether conjugates **12** and **13** activate the same two-component system PfeS/PfeR as Fe-ENT .^{45,46} Periplasmic ferric ENT binds to the PfeS sensor at the inner membrane, activating the transcriptional regulator PfeR, which upregulates the expression of the *pfeA* gene.^{45,46} Induction of *pfeA* transcription in the presence of the conjugates implies that the compounds have crossed the bacterial outer membrane since they can interact with PfeS only in the periplasm. Previous studies have shown that BCV **4** and TCV **5** vectors induce the transcription and expression of *pfeA* and *pfeE*.¹⁶ In the present work *pfeA* and *pfeE* transcriptions are stronger with TCV than with BCV, suggesting that either more TCV is transported than BCV or that the PfeS binding site has a preference for the geometry of the Fe^{3+} -TCV complex rather than that of the Fe^{3+} -BCV complex. RT-qPCR analysis revealed that TCV conjugates **10** and **11** induced *pfeA* and *pfeE* transcription, indicating transport (Figure 7). Thus, the

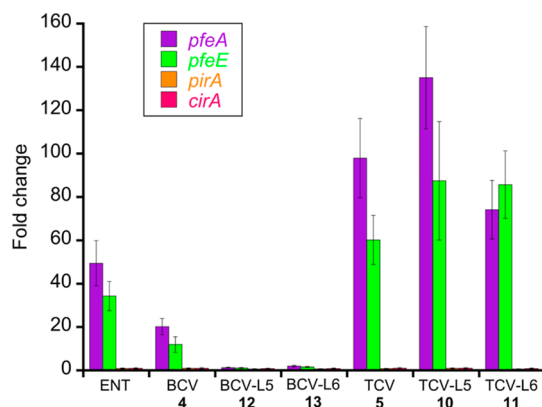


Figure 7. Analysis of changes in the transcription of the TBDDT genes. RT-qPCR was performed on RNA from *P. aeruginosa* PAO1 cells grown in CAA medium, with and without supplementation with 10 μM ENT, BCV, TCV, or conjugates **10** to **13**. The data are normalized relative to the reference gene *uvrD* and are representative of three independent experiments performed in triplicate ($n = 3$). *pfeA* encodes for the TBDDT of ENT, *pfeE* for the esterase involved in ENT hydrolyses, and *pirA* and *cirA* for TBDDT involved in iron acquisition by catechol siderophores.

payload has not prevented transport into the periplasm or binding to the sensor. The induction of *pfeA* and *pfeE* transcription by TCV **5** and its conjugates **10** and **11** appeared stronger than the induction by ENT itself, a fact we attribute to the non-hydrolyzable TCV **5** scaffold by PfeE.¹⁶ Ferric complexes of TCV **5** and of TCV–oxazolidinone conjugates **10** and **11** accumulate in the bacterial periplasm, leading to a sustained stimulation of the sensor, but they do not cross the inner membrane to inhibit the ribosome. In contrast, although BCV **4** induces the expression of the main proteins of the ENT pathway, it is weaker than the natural siderophore ENT and the TCV.³⁹ The BCV–oxazolidinone conjugates **12** and **13** show no induction of *pfeA* and *pfeE* and either are not transported or do not bind to PfeS. Neither ENT, TCV, and BCV nor their conjugates induced the expression of CirA and PirA, two TBDDTs previously described to be involved in the uptake of catechol siderophore and related conjugates (Figure 7).^{40,58}

CONCLUSIONS

Catechol siderophores are used to access iron by many bacterial species, even those unable to produce them. This predominance appears to be related to the extremely high affinity of catechol siderophores for iron in comparison to other natural chelators, yielding a selective advantage in the competition for iron.⁵⁹ *P. aeruginosa* does not produce ENT but can use it as a siderophore by expressing PfeA, a dedicated outer-membrane transporter and PfeE, a periplasmic esterase involved in the hydrolysis of the trilactone ring to facilitate iron release. These two proteins have their expression induced when *P. aeruginosa* is grown in the presence of ENT. Several research groups developed cargo based on the ENT or closely related molecule (salmochelins) to efficiently deliver antibiotic and other xenobiotics into Gram-negative bacteria.^{18,23,32,33} BCV 4 and TCV 5, alternative ENT vectors used in the present study, are easy to prepare on the gram scale and chemically stable compared to the trilactone core of the native siderophore. Moreover, the terminal alkyne of these vectors is a versatile chemical function to the conjugation of a broad range of linkers and payloads. We report here the synthesis of their conjugates 10 to 13 with an oxazolidinone antibiotic. These conjugates proved to be invaluable molecular tools to investigate, for the first time, the recognition process by the specific outer membrane transporter PfeA and the signaling induced across the transporter to get the uptake of the compounds through the bacterial outer membrane. The BCV vector 4 was shown to mimic ENT in the PfeA first binding site, but the related conjugates failed to activate the two-component system PfeS/PfeR located in the inner membrane and involved in the regulation of *pfeA* transcription. However, TCV 5 as a vector in Trojan horse strategies against *P. aeruginosa* showed more promise; both the ferric-vector and the ferric-oxazolidinone conjugates bind to PfeA at the same site as ferric ENT and both result in the activation of the PfeS/PfeR system, suggesting that they are transported inside the bacterial periplasm. These are the properties required for a siderophore-based Trojan horse approach. Since the TCV derivatives are able to enter the bacterial periplasm, these conjugates are most suited to deliver antibiotics with periplasmic targets or whose linker specifically breaks down in the periplasm (thus allowing further transport into the cytoplasm).

MATERIALS AND METHODS

Chemicals. ENT and linezolid used as references were purchased from Sigma-Aldrich. BCV 4 and TCV 5 and their respective protected versions 6 and 7 were prepared according to previously described protocols.⁵¹ Linezolid-azide derivatives 8 and 9 were synthesized according to previously described protocols.⁴⁹ Conjugates 10 to 13 were prepared according to procedures described in the [Supporting Information](#).

Structural Biology. PfeA was produced and crystallized as previously described.³⁸ Apo crystals have been cross-linked by diffusion of a 25% glutaraldehyde prior to being soaked for a few hours in the mother liquor containing 5 mM of either Fe³⁺-BCV, Fe³⁺-BCV-L5, Fe³⁺-BCV-L6, Fe³⁺-TCV, Fe³⁺-TCV-L5, or Fe³⁺-TCV-L6. Data were collected at the beamline IO3, IO4, and IO4-1 at Diamond Light Source. Data were processed with XIA2.^{60–64} Structures of the complexes and mutant proteins have been solved using the apo structure.³⁸ Models were adjusted with COOT,⁶⁵ and

refinement was carried out using REFMAC in the CCP4 program suite with TLS (Translation/Libration/Screw) parameters.⁶⁶ ProSMART has been used for refinement. Coordinates and topologies of ligands were generated using PRODRG.⁶⁷ Atomic coordinates and structure factors have been deposited in the Protein Data Bank (5N3C, 6Z33, 7OBW, 6YYS, 6Z2N, and 6Y47). The quality of the structure was checked with MOLPROBITY.⁶⁸ Figures were drawn using PYMOL.⁶⁹

Isothermal Titration Calorimetry. Affinities of PfeA wild-type and mutants for the Fe³⁺-siderophore were measured by ITC using an ITC200 instrument (Microcal) at 25 °C. Titrations were performed using 19 × 2 μL injections of ~450 μM Fe³⁺-siderophore into ~45 μM protein. The heats of dilution measured from the injection of the ligands into the buffer were subtracted, and titration curves were fitted with a one-site binding model using Origin software with and without the N fixed at 1 and cell adjusted to ~30 μM. Determination of thermodynamic parameters is not fully accurate because of the errors in the Fe³⁺ complex, active PfeA concentrations, and non-sigmoidal profile. Fe³⁺-ENT into PfeA titration has been fitted previously with a cooperative two binding site model using AFFINImeter.

Computational Methods. MD simulations were set up such that the PfeA protein was inserted in a phospholipid membrane and fully solvated using the CHARRM-GUI web server.⁷⁰ In particular, the lipid bilayer consists of 233 POPC (1-palmitoyl-2-oleoyl-*sn*-glycero-3-phosphocholine) molecules with *xy* planar dimensions of 100 Å × 100 Å. The whole system was then immersed in an explicit water solution adding KCl ions to match a concentration of 0.15 M. MD trajectories were produced by using the ACEMD software,⁷¹ whereas AMBER14 and the LIPID14 were chosen as the force fields,^{72,73} respectively, for the protein and the lipids. For the explicit solvent, we have used the TIP3P model.⁷⁴ Fe³⁺-ENT complex parameterization was performed using the Metal Center Parameter Builder.⁷⁵ After the initial heating, the system was equilibrated in the NPT ensemble by gradually releasing the constraints that had been initially applied to the protein Cα/Cβ atoms and phosphorus atoms of the lipid head groups. After several stages of equilibration, we performed 300 ns long MD simulations under the NVT ensemble, using as fixed volume the average volume of the last equilibration stage. Pressure and temperature were kept at 1 atm and 310 K using the isotropic Berendsen barostat and the Langevin thermostat, respectively. Electrostatic interactions were computed using the particle mesh Ewald approach, with a cut-off of 9.0 Å for the short-range evaluation in direct space and with frequency set to 2. Non-bonded interactions were addressed with a switch function where the switch-distance was set to 7.5 Å and cut-off at 9.0 Å. In order to accelerate the simulations, mass of hydrogen atoms were scaled to 4 AMU, which allowed an integrating time step of 4 fs. The Cα correlation was computed by using the bio3d package within R,⁷⁶ and a statistical mechanical approach invariant to relative atomic motions known as linear mutual information (LMI),⁵³ ranging from 0 (no correlation or random movements) to 1 (complete correlation or concerted movements). The beneficial side of the LMI over the conventional methods for detecting correlation in protein motions is its invariance to a relative orientation of atomic fluctuations. Due to this property, the LMI captures a more detailed picture of how protein motions are coupled. Moreover, the LMI omits undesired non-linear

correlations and makes a perfect candidate for considering the protein dynamics. The convergence of the LMI was tested by performing a block analysis where the total trajectory was divided into 50 ns windows, and an LMI matrix was calculated for each window. All figures and plots were produced using the VMD⁷⁷ and R⁷⁸ software.

Quantitative Real-Time PCR Assays. The quantitative real-time PCR assay was carried out as described previously.³⁹ The bacteria were first grown in LB medium overnight at 30 °C and then washed and resuspended in casamino acid medium (CAA), which is an iron-restricted medium, having the following composition: 5 g L⁻¹ low-iron CAA (Difco), 1.46 g L⁻¹ K₂HPO₄·3H₂O, and 0.25 g L⁻¹ MgSO₄·7H₂O and grown overnight at 30 °C. Afterward, the bacteria were diluted to an optical density at 600 nm of 0.1 units and grown for 8 h in fresh CAA medium at 30 °C in the absence or presence of 10 μM ENT, vectors, or conjugates. An aliquot of 2.5 × 10⁸ cells from this culture was added to two volumes of RNA protect Bacteria Reagent (Qiagen), and the same protocol was used for RNA extraction as previously described.⁵⁹ 1 μg of total RNA was then reverse-transcribed with the High-Capacity RNA-to-cDNA Kit, in accordance with the manufacturer's instructions (Applied Biosystems). The amounts of specific complementary DNAs were assessed using a StepOne Plus instrument (Applied Biosystems) with Power Sybr Green PCR Master Mix (Applied Biosystems) and the appropriate primers (see Table S4 in the Supporting Information). Primer efficiencies were determined using serially diluted genomic DNA, and the double ΔC_T method was used to analyze qPCR data.

Evaluation of the Antibiotic Activities. Evaluation of the antibiotic activities of the different compounds was carried out in Mueller–Hinton II Broth (MHB) using the two-fold serial dilution method with an inoculum of 10⁵ bacteria per milliliter. The strains used in this assay are *P. aeruginosa* PAO1 and *S. aureus* HG001. Data are reported as minimum inhibitory concentration (MIC), which corresponds to the lowest concentration of antibiotic that inhibits the visible cell growth after an 18 h culture at 37 °C.

■ ASSOCIATED CONTENT

SI Supporting Information

The Supporting Information is available free of charge at <https://pubs.acs.org/doi/10.1021/acsinfecdis.2c00202>.

General considerations for structural biology, computational, chemical, and microbiology experiments; crystallographic data and refinement statistics; comparison of PfeA complex structures; Ligplot diagrams showing PfeA–siderophore interactions; final 2F_O–F_C electron density map; crystal packing of the PfeA–Fe³⁺–TCV–L6 11 complex; PfeA binding sites of the different complexes; comparison of the isothermal calorimetry titrations of the different complexes; raw data of isothermal calorimetry titrations; thermodynamic parameters of the Fe³⁺ siderophore to PfeA; distribution of the Cα correlation strength; molecular graphics of the progression of TCV–L6 11 toward the second binding site of PfeA; MICs measured in MHB medium with *P. aeruginosa* PAO1 and *S. aureus* HG001 strains; primers used for RT-qPCR analysis; experimental procedures for the synthesis of compounds 10 to 13; and ¹H, ¹⁹F, and ¹³C NMR and LC/HRMS spectra of compounds 10 to 13 (PDF)

■ AUTHOR INFORMATION

Corresponding Author

Gaëtan L.A. Mislin – CNRS, UMR7242 Biotechnologie et Signalisation Cellulaire, F-67412 Illkirch, France; Université de Strasbourg, Institut de Recherche de l'École de Biotechnologie de Strasbourg (IREBS), F-67412 Illkirch, France; orcid.org/0000-0002-5646-3392; Email: mislin@unistra.fr

Authors

Lucile Moynié – The Rosalind Franklin Institute, Oxfordshire OX11 0QS, U.K.

Françoise Hoegy – CNRS, UMR7242 Biotechnologie et Signalisation Cellulaire, F-67412 Illkirch, France; Université de Strasbourg, Institut de Recherche de l'École de Biotechnologie de Strasbourg (IREBS), F-67412 Illkirch, France

Stefan Milenkovic – Department of Physics, University of Cagliari, 09042 Monserrato, Italy

Mathilde Munier – CNRS, UMR7242 Biotechnologie et Signalisation Cellulaire, F-67412 Illkirch, France; Université de Strasbourg, Institut de Recherche de l'École de Biotechnologie de Strasbourg (IREBS), F-67412 Illkirch, France

Aurélien Paulen – CNRS, UMR7242 Biotechnologie et Signalisation Cellulaire, F-67412 Illkirch, France; Université de Strasbourg, Institut de Recherche de l'École de Biotechnologie de Strasbourg (IREBS), F-67412 Illkirch, France

Véronique Gasser – CNRS, UMR7242 Biotechnologie et Signalisation Cellulaire, F-67412 Illkirch, France; Université de Strasbourg, Institut de Recherche de l'École de Biotechnologie de Strasbourg (IREBS), F-67412 Illkirch, France

Aline L. Faucon – CNRS, UMR7242 Biotechnologie et Signalisation Cellulaire, F-67412 Illkirch, France; Université de Strasbourg, Institut de Recherche de l'École de Biotechnologie de Strasbourg (IREBS), F-67412 Illkirch, France

Nicolas Zill – CNRS, UMR7242 Biotechnologie et Signalisation Cellulaire, F-67412 Illkirch, France; Université de Strasbourg, Institut de Recherche de l'École de Biotechnologie de Strasbourg (IREBS), F-67412 Illkirch, France

James H. Naismith – The Rosalind Franklin Institute, Oxfordshire OX11 0QS, U.K.; Division of Structural Biology, Wellcome Trust Centre of Human Genomics, Oxford OX3 7BN, U.K.; orcid.org/0000-0001-6744-5061

Matteo Ceccarelli – Department of Physics, University of Cagliari, 09042 Monserrato, Italy; IOM/CNR, Sezione di Cagliari, University of Cagliari, 09042 Monserrato, Italy; orcid.org/0000-0003-4272-902X

Isabelle J. Schalk – CNRS, UMR7242 Biotechnologie et Signalisation Cellulaire, F-67412 Illkirch, France; Université de Strasbourg, Institut de Recherche de l'École de Biotechnologie de Strasbourg (IREBS), F-67412 Illkirch, France; orcid.org/0000-0002-8351-1679

Complete contact information is available at:

<https://pubs.acs.org/doi/10.1021/acsinfecdis.2c00202>

Author Contributions

G.L.A.M., L.M., I.J.S., J.H.N., and M.C. wrote the manuscript with inputs from the others. L.M. performed structural biology

and biophysic analysis. F.H., N.Z., A.P., M.M., and A.L.F. designed the target molecules, did the chemical experiments, purified, and characterized compounds **10** to **13** and their synthetic precursors. V.G. performed antibiotic assays and qRT-PCR experiments. I.J.S. supervised the microbiology experiments. S.M. designed, performed, and analyzed the MD simulations. I.J.S., G.L.A.M., M.C., and J.H.N. obtained the grants.

Notes

The authors declare no competing financial interest.

ACKNOWLEDGMENTS

G.L.A.M. and I.J.S. warmly thank Vaincre la Mucoviscidose and the Association Grégory Lemarchal (French associations against cystic fibrosis) for repeated financial support. G.L.A.M. acknowledges the Agence Nationale pour la Recherche (VECTRIUM project, ANR 19-CE18-0011-02) for financial support and for a Ph.D. fellowship attributed to A.L.F. G.L.A.M. and I.J.S. also acknowledge the Interdisciplinary Thematic Institute (ITI) InnoVec (Innovative Vectorization of Biomolecules, IdEx, ANR-10-IDEX-0002) and SFRI (ANR-20-SFRI-0012). A.P. acknowledges the Ministère de l'Éducation Nationale, de l'Enseignement Supérieur et de la Recherche (MENESR) for a PhD fellowship. Authors also acknowledge the Centre National de la Recherche Scientifique (CNRS) for general financial support. L.M., S.M., M.M., and N.Z. acknowledge the Translocation consortium for their post-doctoral fellowships: the research leading to these results was conducted as part of the Translocation consortium (www.translocation.com) and benefited from support from ND4BB ENABLE. All teams involved in the present work have received support from the Innovative Medicines Joint Undertaking under grant agreement nos 115525 and 115583, resources which are composed of financial contributions from the European Union's seventh framework program (FP7/2007-2013) and EFPIA companies in kind contribution. Finally, the authors acknowledge the Institut National de la Santé et de la Recherche Médicale (INSERM) and AstraZeneca for granting the AnBRe project (IMMI_2014014). This work is supported by a Wellcome Trust Investigator (100209/Z/12/Z) award. M.C. and S.M. would like to thank Giuliano Mallocci for providing the AMBER topology for the simulated molecules. M.C. thanks computer facilities at CINECA provided by the project "IscrB_PREDICT". Work at the Rosalind Franklin Institute was supported by core funding by EPSRC. We would like to thank the Membrane Protein Laboratory at Diamond Light (funded by Wellcome Trust grant 223727/Z/21/Z) for help and support.

REFERENCES

- (1) Murphy, T. F. Editorial Commentary: The Many Faces of *Pseudomonas aeruginosa* in Chronic Obstructive Pulmonary Disease. *Clin. Infect. Dis.* **2008**, *47*, 1534–1536.
- (2) Folkesson, A.; Jelsbak, L.; Yang, L.; Johansen, H. K. O.; Ciofu, N.; Høiby, S.; Molin, S. Adaptation of *Pseudomonas aeruginosa* to the cystic fibrosis airway: an evolutionary perspective. *Nat. Rev. Microbiol.* **2012**, *10*, 841–851.
- (3) Schuster, M.; Norris, A. Community-acquired *Pseudomonas aeruginosa* pneumonia in patients with HIV infection. *AIDS* **1994**, *8*, 1437–1442.
- (4) Church, D.; Elsayed, S.; Reid, O.; Winston, B.; Lindsay, R. Burn wound infections. *Clin. Microbiol. Rev.* **2006**, *19*, 403–434.
- (5) Nikaido, H. Molecular basis of bacterial outer membrane permeability revisited. *Microbiol. Mol. Biol. Rev.* **2003**, *67*, 593–656.

- (6) Raymond, K. N.; Carrano, C. J. Coordination chemistry and microbial iron transport. *Acc. Chem. Res.* **1979**, *12*, 183–190.
- (7) Braun, V.; Killmann, H. Bacterial solutions to the iron-supply problem. *Trends Biochem. Sci.* **1999**, *24*, 104–109.
- (8) Cornelis, P.; Dingemans, J. *Pseudomonas aeruginosa* adapts its iron uptake strategies in function of the type of infections. *Front. Cell. Infect. Microbiol.* **2013**, *3*, 75.
- (9) Hider, R. C.; Kong, X. Chemistry and biology of siderophores. *Nat. Prod. Rep.* **2010**, *27*, 637–657.
- (10) Moynié, L.; Serra, I.; Scorciapino, M. A.; Oueis, E.; Page, M. G.; Ceccarelli, M.; Naismith, J. H. Preacinetobactin not acinetobactin is essential for iron uptake by the BauA transporter of the pathogen *Acinetobacter baumannii*. *Elife* **2018**, *7*, No. e42270.
- (11) Schalk, I. J.; Mislin, G. L. A.; Brillet, K. Structure, function and binding selectivity and stereoselectivity of siderophore-iron outer membrane transporters. *Curr. Top. Membr.* **2012**, *69*, 37–66.
- (12) Klebba, P. E.; Newton, S. M. C.; Six, D. A.; Kumar, A.; Yang, T.; Nairn, B. L.; Munger, C.; Chakravorty, S. Iron Acquisition Systems of Gram-negative Bacterial Pathogens Define TonB-Dependent Pathways to Novel Antibiotics. *Chem. Rev.* **2021**, *121*, 5193–5239.
- (13) Noinaj, N.; Guillier, M.; Barnard, T. J.; Buchanan, S. K. TonB-dependent transporters: regulation, structure, and function. *Annu. Rev. Microbiol.* **2010**, *64*, 43–60.
- (14) Celia, H.; Noinaj, N.; Zakharov, S. D.; Bordignon, E.; Botos, I.; Santamaria, M.; Barnard, T. J.; Cramer, W. A.; Lloubes, R.; Buchanan, S. K. Structural insight into the role of the Ton complex in energy transduction. *Nature* **2016**, *538*, 60–65.
- (15) Schalk, I. J.; Guillon, L. Fate of ferrisiderophores after import across bacterial outer membranes: different iron release strategies are observed in the cytoplasm or periplasm depending on the siderophore pathways. *Amino Acids* **2013**, *44*, 1267–1277.
- (16) Perraud, Q.; Moynié, L.; Gasser, V.; Munier, M.; Godet, J.; Hoegy, F.; Mély, Y.; Mislin, G. L. A.; Naismith, J. H.; Schalk, I. J. A Key Role for the Periplasmic PfeE Esterase in Iron Acquisition via the Siderophore Enterobactin in *Pseudomonas aeruginosa*. *ACS Chem. Biol.* **2018**, *13*, 2603–2614.
- (17) Mislin, G. L. A.; Schalk, I. J. Siderophore-dependent iron uptake systems as gates for antibiotic Trojan horse strategies against *Pseudomonas aeruginosa*. *Metallomics* **2014**, *6*, 408–420.
- (18) Neumann, W.; Sassone-Corsi, M.; Raffatellu, M.; Nolan, E. M. Esterase-catalyzed siderophore hydrolysis activates an enterobactin-ciprofloxacin conjugate and confers targeted antibacterial activity. *J. Am. Chem. Soc.* **2018**, *140*, 5193–5201.
- (19) Fardeau, S.; Dassonville-Klimpt, A.; Audic, N.; Sasaki, A.; Pillon, M.; Baudrin, E.; Mullié, C.; Sonnet, P. Synthesis and antibacterial activity of catecholate-ciprofloxacin conjugates. *Bioorg. Med. Chem.* **2014**, *22*, 4049–4060.
- (20) Ji, C.; Miller, P. A.; Miller, M. J. Iron Transport-Mediated Drug Delivery: Practical Syntheses and In Vitro Antibacterial Studies of Tris-Catecholate Siderophore-Aminopenicillin Conjugates Reveals Selectively Potent Antipseudomonal Activity. *J. Am. Chem. Soc.* **2012**, *134*, 9898–9901.
- (21) Möllmann, U.; Heinisch, L.; Bauernfeind, A.; Köhler, T.; Ankel-Fuchs, D. Siderophores as drug delivery agents: application of the "Trojan Horse" strategy. *BioMetals* **2009**, *22*, 615–624.
- (22) Milner, S. J.; Seve, A.; Snelling, A. M.; Thomas, G. H.; Kerr, K. G.; Routledge, A.; Duhme-Klair, A.-K. Staphyloferrin A as siderophore-component in fluoroquinolone-based Trojan horse antibiotics. *Org. Biomol. Chem.* **2013**, *11*, 3461–3468.
- (23) Sanderson, T. J.; Black, C. M.; Southwell, J. W.; Wilde, E. J.; Pandey, A.; Herman, R.; Thomas, G. H.; Boros, E.; Duhme-Klair, A.-K.; Routledge, A. A Salmochelin S4-Inspired Ciprofloxacin Trojan Horse Conjugate. *ACS Infect. Dis.* **2020**, *6*, 2532–2541.
- (24) Scorciapino, M. A.; Mallocci, G.; Serra, I.; Milenkovic, S.; Moynié, L.; Naismith, J. H.; Desarbre, E.; Page, M. G.; Ceccarelli, M. Complexes formed by the siderophore-based monosulfactam antibiotic BAL30072 and their interaction with the outer membrane receptor PiuA of *P. aeruginosa*. *BioMetals* **2019**, *32*, 155–170.

- (25) de Carvalho, C. C. C. R.; Fernandes, P. Siderophores as “Trojan Horses”: tackling multidrug resistance? *Front. Microbiol.* **2014**, *5*, 290.
- (26) Kong, H.; Cheng, W.; Wei, H.; Yuan, Y.; Yang, Z.; Zhang, X. An overview of recent progress in siderophore-antibiotic conjugates. *Eur. J. Med. Chem.* **2019**, *182*, 111615.
- (27) Negash, K. H.; Norris, J. K. S.; Hodgkinson, J. T. Siderophore-Antibiotic Conjugate Design: New Drugs for Bad Bugs? *Molecules* **2019**, *24*, 3314.
- (28) Lin, Y. M.; Ghosh, M.; Miller, P. A.; Möllmann, U.; Miller, M. J. Synthetic sideromycins (skepticism and optimism): selective generation of either broad or narrow spectrum Gram-negative antibiotics. *BioMetals* **2019**, *32*, 425–451.
- (29) Górska, A.; Sloderbach, A.; Marszał, M. P. Siderophore-drug complexes: potential medicinal applications of the “Trojan horse” strategy. *Trends Pharmacol. Sci.* **2014**, *35*, 442–449.
- (30) Liu, R.; Miller, P. A.; Miller, M. J. Conjugation of Aztreonam, a Synthetic Monocyclic β -Lactam Antibiotic, to a Siderophore Mimetic Significantly Expands Activity Against Gram-Negative Bacteria. *ACS Infect. Dis.* **2021**, *7*, 2979–2986.
- (31) Pinkert, L.; Lai, Y. H.; Peukert, C.; Hotop, S. K.; Karge, B.; Schulze, L. M.; Grunenberg, J.; Brönstrup, M. Antibiotic Conjugates with an Artificial MECAM-Based Siderophore Are Potent Agents against Gram-Positive and Gram-Negative Bacterial Pathogens. *J. Med. Chem.* **2021**, *64*, 15440–15460.
- (32) Zscherp, R.; Coetzee, J.; Vornweg, J.; Grunenberg, J.; Herrmann, J.; Müller, R.; Klahn, P. Biomimetic enterobactin analogue mediates iron-uptake and cargo transport into *E. coli* and *P. aeruginosa*. *Chem. Sci.* **2021**, *12*, 10179–10190.
- (33) Klahn, P.; Zscherp, R.; Jimidar, C. C. Advances in the Synthesis of Enterobactin, Artificial Analogues, and Enterobactin-Derived Antimicrobial Drug Conjugates and Imaging Tools for Infection Diagnosis. *Synthesis* **2022**, DOI: 10.1055/a-1783-0751. , in press.
- (34) Raymond, K. N.; Dertz, E. A.; Kim, S. S. Enterobactin: an archetype for microbial iron transport. *Proc. Natl. Acad. Sci. U.S.A.* **2003**, *100*, 3584–3588.
- (35) Cox, C. D.; Rinehart, K. L., Jr.; Moore, M. L.; Cook, J. C., Jr. Pyochelin: novel structure of an iron-chelating growth promoter for *Pseudomonas aeruginosa*. *Proc. Natl. Acad. Sci. U.S.A.* **1981**, *78*, 4256–4260.
- (36) Abdallah, M. A.; Pfestorf, M.; Döring, G. *Pseudomonas aeruginosa* pyoverdinin: structure and function. *Antibiot. Chemother.* **1989**, *42*, 8–14.
- (37) Dean, C. R.; Poole, K. Expression of the ferric enterobactin receptor (PfeA) of *Pseudomonas aeruginosa*: involvement of a two-component regulatory system. *Mol. Microbiol.* **1993**, *8*, 1095–1103.
- (38) Moynié, L.; Milenkovic, S.; Mislin, G. L. A.; Gasser, V.; Mallocci, G.; Baco, E.; McCaughan, R. P.; Page, M. G. P.; Schalk, I. J.; Ceccarelli, M.; Naismith, J. H. The complex of ferric-enterobactin with its transporter from *Pseudomonas aeruginosa* suggests a two-site model. *Nat. Commun.* **2019**, *10*, 3673.
- (39) Gasser, V.; Baco, E.; Cunrath, O.; August, P.; Perraud, Q.; Zill, N.; Schleberger, C.; Schmidt, A.; Paulen, A.; Bumann, D.; Mislin, G. L. A.; Schalk, I. J. Catechol siderophores repress the pyochelin pathway and activate the enterobactin pathway in *Pseudomonas aeruginosa*: an opportunity for siderophore-antibiotic conjugates development. *Environ. Microbiol.* **2016**, *18*, 819–832.
- (40) Ghysels, B.; Ochsner, U.; Möllman, U.; Heinisch, L.; Vasil, M.; Cornelis, P.; Matthijs, S. The *Pseudomonas aeruginosa* *pirA* Gene Encodes a Second Receptor for Ferrienterobactin and Synthetic Catecholate Analogues. *FEMS Microbiol. Lett.* **2005**, *246*, 167–174.
- (41) Gasser, V.; Kuhn, L.; Hubert, T.; Aussel, L.; Hammann, P.; Schalk, I. J. The Esterase PfeE, the Achilles’ Heel in the Battle for Iron between *Pseudomonas aeruginosa* and *Escherichia coli*. *Int. J. Mol. Sci.* **2021**, *22*, 2814.
- (42) Brickman, T. J.; McIntosh, M. A. Overexpression and Purification of Ferric Enterobactin Esterase from *Escherichia coli*. Demonstration of Enzymatic Hydrolysis of Enterobactin and Its Iron Complex. *J. Biol. Chem.* **1992**, *267*, 12350–12355.
- (43) Lin, H.; Fischbach, M. A.; Liu, D. R.; Walsh, C. T. In Vitro Characterization of Salmochelin and Enterobactin Trilactone Hydro-lases IroD, IroE, and Fes. *J. Am. Chem. Soc.* **2005**, *127*, 11075–11084.
- (44) Miethke, M.; Hou, J.; Marahiel, M. A. The Siderophore-Interacting Protein YqjH Acts as a Ferric Reductase in Different Iron Assimilation Pathways of *Escherichia coli*. *Biochemistry* **2011**, *50*, 10951–10964.
- (45) Dean, C. R.; Neshat, S.; Poole, K. PfeR, an enterobactin-responsive activator of ferric enterobactin receptor gene expression in *Pseudomonas aeruginosa*. *J. Bacteriol.* **1996**, *178*, 5361–5369.
- (46) Crosa, J. H. Signal Transduction and Transcriptional and Posttranscriptional Control of Iron-Regulated Genes in Bacteria. *Microbiol. Mol. Biol. Rev.* **1997**, *61*, 319–336.
- (47) Josts, I.; Veith, K.; Tidow, H. Ternary structure of the outer membrane transporter FoxA with resolved signalling domain provides insights into TonB-mediated siderophore uptake. *Elife* **2019**, *8*, No. e48528.
- (48) Grinter, R.; Lithgow, T. The structure of the bacterial iron-catecholate transporter Fiu suggests that it imports substrates via a two-step mechanism. *J. Biol. Chem.* **2019**, *294*, 19523–19534.
- (49) Paulen, A.; Gasser, V.; Hoegy, F.; Perraud, Q.; Pesset, B.; Schalk, I. J.; Mislin, G. L. A. Synthesis and antibiotic activity of oxazolidinone-catechol conjugates against *Pseudomonas aeruginosa*. *Org. Biomol. Chem.* **2015**, *13*, 11567–11579.
- (50) Liu, R.; Miller, P. A.; Vakulenko, S. B.; Stewart, N. K.; Boggess, W. C.; Miller, M. J. A Synthetic Dual Drug Sideromycin Induces Gram-Negative Bacteria To Commit Suicide with a Gram-Positive Antibiotic. *J. Med. Chem.* **2018**, *61*, 3845–3854.
- (51) Baco, E.; Hoegy, F.; Schalk, I. J.; Mislin, G. L. A. Diphenylbenzo[1,3]dioxole-4-carboxylic acid pentafluorophenyl ester: a convenient catechol precursor in the synthesis of siderophore vectors suitable for antibiotic Trojan horse strategies. *Org. Biomol. Chem.* **2014**, *12*, 749–757.
- (52) Ichiye, T.; Karplus, M. Collective motions in proteins: A covariance analysis of atomic fluctuations in molecular dynamics and normal mode simulations. *Proteins* **1991**, *11*, 205–217.
- (53) Lange, O. F.; Grubmüller, H. Generalized correlation for biomolecular dynamics. *Proteins* **2006**, *62*, 1053–1061.
- (54) Paulen, A.; Hoegy, F.; Roche, B.; Schalk, I. J.; Mislin, G. L. A. Synthesis of conjugates between oxazolidinone antibiotics and a pyochelin analogue. *Bioorg. Med. Chem. Lett.* **2017**, *27*, 4867–4870.
- (55) Rostovtsev, V. V.; Green, L. G.; Fokin, V. V.; Sharpless, K. B. A Stepwise Huisgen Cycloaddition Process: Copper(I)-Catalyzed Regioselective “Ligation” of Azides and Terminal Alkynes. *Angew. Chem., Int. Ed. Engl.* **2002**, *41*, 2596–2599.
- (56) Tornøe, C. W.; Christensen, C.; Meldal, M. Peptidotriazoles on Solid Phase: [1,2,3]-Triazoles by Regiospecific Copper(I)-Catalyzed 1,3-Dipolar Cycloadditions of Terminal Alkynes to Azides. *J. Org. Chem.* **2002**, *67*, 3057–3064.
- (57) Bozdoğan, B.; Appelbaum, P. C. Oxazolidinones: activity, mode of action, and mechanism of resistance. *Int. J. Antimicrob. Agents* **2004**, *23*, 113–119.
- (58) Luscher, A.; Moynié, L.; Auguste, P.; Bumann, D.; Mazza, L.; Pletzer, D.; Naismith, J. H.; Köhler, T. TonB-Dependent Receptor Repertoire of *Pseudomonas aeruginosa* for Uptake of Siderophore-Drug Conjugates. *Antimicrob. Agents Chemother.* **2018**, *62*, No. e00097.
- (59) Perraud, Q.; Cantero, P.; Roche, B.; Gasser, V.; Normant, V. P.; Kuhn, L.; Hammann, P.; Mislin, G. L. A.; Ehret-Sabatier, L.; Schalk, I. J. Phenotypic adaptation of *Pseudomonas aeruginosa* by hacking siderophores produced by other microorganisms. *Mol. Cell. Proteomics* **2020**, *19*, 589–607.
- (60) Winter, G. xia2: an expert system for macromolecular crystallography data reduction. *J. Appl. Crystallogr.* **2010**, *43*, 186–190.
- (61) Zhang, Z.; Sauter, N. K.; van den Bedem, H.; Snell, G.; Deacon, A. M. Automated diffraction image analysis and spot searching for high-throughput crystal screening. *J. Appl. Crystallogr.* **2006**, *39*, 112–119.

(62) Sauter, N. K.; Grosse-Kunstleve, R. W.; Adams, P. D. Robust indexing for automatic data collection. *J. Appl. Crystallogr.* **2004**, *37*, 399–409.

(63) Kabsch, W. Automatic Processing of Rotation Diffraction Data from Crystals of Initially Unknown Symmetry and Cell Constants. *J. Appl. Crystallogr.* **1993**, *26*, 795–800.

(64) Evans, P. Scaling and assessment of data quality. *Acta Crystallogr. D* **2006**, *62*, 72–82.

(65) Emsley, P.; Cowtan, K. Coot: model-building tools for molecular graphics. *Acta Crystallogr. D* **2004**, *60*, 2126–2132.

(66) Murshudov, G. N.; Vagin, A. A.; Dodson, E. J. Refinement of macromolecular structures by the maximum-likelihood method. *Acta Crystallogr. Sect. D Biol. Crystallogr.* **1997**, *53*, 240–255.

(67) Schüttelkopf, A. W.; van Aalten, D. M. PRODRG: a tool for high-throughput crystallography of protein-ligand complexes. *Acta Crystallogr. Sect. D Biol. Crystallogr.* **2004**, *60*, 1355–1363.

(68) Chen, V. B.; Arendall, W. B., 3rd; Headd, J. J.; Keedy, D. A.; Immormino, R. M.; Kapral, G. J.; Murray, L. W.; Richardson, J. S.; Richardson, D. C. MolProbity: all-atom structure validation for macromolecular crystallography. *Acta Crystallogr. Sect. D Biol. Crystallogr.* **2010**, *66*, 12–21.

(69) Schrodinger, LLC *The PyMOL Molecular Graphics System*, 2010 version.

(70) Jo, S.; Kim, T.; Iyer, V. G. W.; Im, W. CHARMM-GUI: A web-based graphical user interface for CHARMM. *J. Comput. Chem.* **2008**, *29*, 1859–1865.

(71) Harvey, M. J.; Giupponi, G.; Fabritiis, G. ACEMD: accelerating biomolecular dynamics in the microsecond time scale. *J. Chem. Theory Comput.* **2009**, *5*, 1632–1639.

(72) Dickson, C. J.; Madej, B. D.; Skjevik, Å.A.; Betz, R. M.; Teigen, K.; Gould, I. R.; Walker, R. C. Lipid14: the amber lipid force field. *J. Chem. Theory Comput.* **2014**, *10*, 865–879.

(73) Maier, J. A.; Martinez, C.; Kasavajhala, K.; Wickstrom, L.; Hauser, K. E.; Simmerling, C. ff14SB: Improving the accuracy of protein side chain and backbone parameters from ff99SB. *J. Chem. Theory Comput.* **2015**, *11*, 3696–3713.

(74) Jorgensen, W. L.; Chandrasekhar, J.; Madura, J. D.; Impey, R. W.; Klein, M. L. Comparison of simple potential functions for simulating liquid water. *J. Chem. Phys.* **1983**, *79*, 926–935.

(75) Li, P.; Merz, K. M., Jr. MCPB.py: A python based metal center parameter builder. *J. Chem. Inf. Model.* **2016**, *56*, 599–604.

(76) Grant, B. J.; Rodrigues, A. P. C.; ElSawy, K. M.; McCammon, J. A.; Caves, L. S. D. Bio3d: an R package for the comparative analysis of protein structures. *Bioinformatics* **2006**, *22*, 2695–2696.

(77) William, H.; Dalke, A.; Schulten, K. VMD: Visual molecular dynamics. *J. Mol. Graph.* **1996**, *14*, 33–38.

(78) R Core Team *Language Definition*; R foundation for statistical computing: Vienna, Austria, 2000.

Recommended by ACS

Uptake Mechanisms and Regulatory Responses to MECAM- and DOTAM-Based Artificial Siderophores and Their Antibiotic Conjugates in *Pseudomonas aer...*

Sarah Fritsch, Isabelle J. Schalk, *et al.*

MAY 02, 2022
ACS INFECTIOUS DISEASES

READ 

Modular Synthetic Routes to Fluorine-Containing Halogenated Phenazine and Acridine Agents That Induce Rapid Iron Starvation in Methicillin-Resistan...

Ke Liu, Robert W. Huigens III, *et al.*

JANUARY 28, 2022
ACS INFECTIOUS DISEASES

READ 

Exotoxin-Targeted Drug Modalities as Antibiotic Alternatives

Moona Sakari, Arto T. Pulliainen, *et al.*

JANUARY 31, 2022
ACS INFECTIOUS DISEASES

READ 

Two plus One: Combination Therapy Tri-systems Involving Two Membrane-Disrupting Antimicrobial Macromolecules and Antibiotics

Zeyu Shao, Edgar H. H. Wong, *et al.*

JUNE 30, 2022
ACS INFECTIOUS DISEASES

READ 

Get More Suggestions >